Functionalized Surface-Confined Pores: Guest Binding Directed by Lateral Noncovalent Interactions at the Solid–Liquid Interface

Kazukuni Tahara,[†,‡,*] Keisuke Katayama,[†] Matthew Oliver Blunt,[§] Kohei Iritani,[†] Steven De Feyter,[§,*] and Yoshito Tobe[†,*]

[†]Division of Frontier Materials Science, Graduate School of Engineering Science, Osaka University, Toyonaka, Osaka 560-8531, Japan, [‡]PRESTO, Japan Science and Technology Agency (JST), Toyonaka, Osaka 560-8531, Japan, and [§]Division of Molecular Imaging and Photonics, Department of Chemistry, KU Leuven, 3001 Leuven, Belgium

ABSTRACT We present here the construction of self-assembled two-dimensional (2D) molecular networks that contain pores equipped with functional groups that promote guest-specific binding at the liquid/solid interface. For this purpose, a dehydrobenzo[12]annulene (DBA) derivative, DBA-F, having perfluoroalkyl groups at the end of the three alternating alkoxy chains connected by *para*-phenylene linkers was synthesized. For comparison DBA-H, having the same carbon backbone without fluorine substituents, was also prepared. STM observations revealed that these molecules formed porous 2D networks whose pores were decorated with either fluoroalkane or simple alkane perimeters. Hexakis-(phenylethynyl)benzene, HPEB, and its octadecafluoro derivative, HPEB-F surrounded by 18 fluorine atoms, were employed as planar guest molecules of suitable size. The fluoroalkane-lined pores present in the network of DBA-F exhibited good binding ability toward both guest molecules *via* fluorophilicity and electrostatic interaction, respectively. In contrast the binding ability of the alkane-lined pore of the network of DBA-H for the fluorinated guest HPEB-F was poor as a result of weaker electrostatic interaction. Interestingly, with HPEB as a guest, this network underwent a periodical structural deformation through an induced-fit mechanism to form a superlattice structure consisting of free and occupied pores. These observations are discussed based on modeling experiments using molecular mechanics and quantum chemical methods to elucidate the roles of lateral noncovalent interactions and size matching between the pore and the guest molecules used for 2D guest binding.

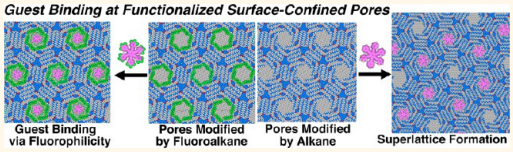

KEYWORDS: self-assembly · solid–liquid interface · scanning tunneling microscopy · porous network · fluorophilicity

Two-dimensional (2D) molecular networks formed by the self-assembly of organic molecules on solid surfaces have attracted a great deal of interest because of their promising use as functional surfaces.[1−5] Among various molecular networks, the construction of 2D porous molecular networks has become a subject of intense activity due to the ability of surface-confined pores (nanowells) in these networks to accommodate guest molecules and thereby act as templates for the construction of multicomponent 2D nanostructures.[6−9] The main driving forces for this phenomenon are vertical van der Waals interactions between a guest and the solid substrate surface and lateral van der Waals interactions between a guest and the surrounding host matrix of the molecular network. For these lateral interactions, shape and size complementarity between the guest and the pore play an important role. Such molecular networks are typically observed by means of scanning tunneling microscopy (STM) under ultrahigh vacuum conditions or at a liquid–solid interface.

One of the most significant challenges in this field is the modification of the chemical environment in the interior space of 2D pores. A few reports have demonstrated the modification of 2D pores with space-controlling groups that recognize the size and shape of guest molecules.[10−14] However, the construction of 2D pores equipped with functional groups that have a binding ability that targets specific neutral guest molecules *via* polar noncovalent interactions has scarcely been achieved. Ion–dipole interactions have previously been exploited to switch or modulate the structures of

* Address correspondence to tahara@chem.es.osaka-u.ac.jp, steven.defeyter@chem.kuleuven.be, tobe@chem.es.osaka-u.ac.jp.

Received for review July 11, 2014 and accepted August 4, 2014.

Published online August 04, 2014
10.1021/nn503815q

molecular networks with binding sites for alkali metal ions or protons.[15−17] With regard to on-surface binding of guest molecules by ion−dipole interactions, only example is a pyridine-based macrocycle having a covalently bonded pore.[18] No polar-functionalized pores formed by self-assembly through noncovalent interactions have been reported. In this context, investigation into the guest binding ability of such functionalized 2D pores is an important subject that has the potential to advance the utility of self-assembled monolayers as functional nanostructures.

Here we delineate the construction of surface-confined pores that are outlined with fluoroalkane groups as a model to investigate the effect of noncovalent interactions exerted by this functionalization on 2D guest binding. It is well-known that homogeneous mixing of liquid alkanes and fluoroalkanes is highly disfavored due to the inequality of the cohesive energy densities.[19−25] Moreover, fluorinated parts in molecules tend to aggregate by themselves, often showing phase segregation at the supramolecular level.[26] This unique behavior has been utilized in the design of molecular self-assemblies such as liquid-crystalline materials,[27−30] one-dimensional columns,[31] and lipid bilayers.[32] Moreover, this character has also been exploited for host−guest interactions: fluoroalkanes were entrapped in a fluorous environment constructed within the interior of metal organic frameworks.[33] However, contrary to many reports in three-dimensional systems such unique behavior of molecules containing fluoroalkyl groups has not been reported in 2D self-assembled monolayers. For example, in the monolayers formed by phthalic acid derivatives having a partially fluorinated alkyl chain, phase separation was not observed as stable phases because of a compromise of repulsive and attractive interactions.[34,35] In addition, the use of a fluorous environment to promote guest binding in a 2D surface-confined pore has never been reported.

For construction of a fluoroalkane-lined 2D pore, a dehydrobenzo[12]annulene (DBA) derivative having six alkoxy chains was chosen as a basic molecular building block. We have previously reported that DBAs form porous honeycomb structures at the liquid/solid interfaces by van der Waals interactions between interdigitated alkyl chains attached to adjacent molecules.[36−39] Moreover, the pore environment can be modified through the introduction of functional groups at the end of three of the six alkyl chains of a DBA molecule in an alternating fashion.[14] To this end, we designed and synthesized **DBA-F**, having perfluoroalkyl groups at the end of the three alkoxy chains connected with *para*-phenylene linkers (Figure 1a). In addition, **DBA-H**, having alkyl groups instead of the perfluoroalkyl groups, was synthesized as a reference compound. Molecular modeling predicted that both DBAs would form honeycomb structures in which the fluoroalkyl or alkyl groups are positioned around the perimeter of the hexagonal pores (Figure 1b,c). To examine the guest binding abilities of the modified pores, we designed and synthesized two planar guest molecules: hexakis(phenylethynyl)benzene **HPEB** and its octadecafluoro derivative **HPEB-F**. These guest molecules were chosen because of the match in terms of both shape and size with the hexagonal pores of the DBA networks. For **HPEB-F**, the outer edge of the guest molecule is decorated with 18 fluorine atoms.

STM observations of monolayers formed by **DBA-F** and **DBA-H** at a liquid/solid interface revealed the formation of honeycomb structures in which the fluoroalkyl or alkyl groups are positioned around the perimeter of the hexagonal pores. The guest binding abilities of these modified pores were evaluated using **HPEB-F** and **HPEB**, revealing that fluorophilicity and H···F electrostatic interactions between the guest and the (fluoro)alkane groups decorating the 2D pores play a crucial role. This is, to our knowledge, the first example of the use of such interactions in 2D guest binding. Moreover, we unexpectedly found the formation of a superlattice structure in the combination of **DBA-H** and **HPEB** *via* an induced-fit mechanism resulting from the adaptability of the host molecular network. Finally, we discuss these observations on the basis of modeling experiments using molecular mechanics (MM) simulations and quantum chemical calculations.

RESULTS

Experimental Details. The synthesis of **DBA-F** and **DBA-H** was conducted based on a previously reported method (see Supporting Information).[14,40] Self-assembled monolayers were prepared by dropping a solution of compound(s) in 1-phenyloctane (*ca.* 8 μL) onto a graphite surface. All STM observations of the monolayers were performed at the interface between 1-phenyloctane and graphite at room temperature. The solute concentration of DBAs was set to less than 4.4×10^{-6} M to ensure the formation of the porous honeycomb structures.[37,38] Mixtures of a DBA (3.1×10^{-6} M) and an appropriate guest molecule (1.3×10^{-6} M) in 1-phenyloctane (25 μL) were poured into a liquid cell placed on the graphite substrate, and these setups were annealed at 70 °C for 30 min in a sealed oven before carrying out the STM imaging to explore guest binding experiments.

STM Observation of Porous Molecular Networks Formed by DBA-F and DBA-H. Figure 2a,b displays an STM image and a molecular model of the 2D molecular network formed by **DBA-F** at the 1-phenyloctane/graphite interface. In the STM image, the bright features correspond to the conjugated cores of **DBA-F**, and the darker parts are composed of four interdigitated alkyl chains,[41] revealing the formation of a honeycomb structure. The orientations of the four interdigitated alkyl chains are parallel to the main symmetry axes of the underlying graphite surface. Small bright single

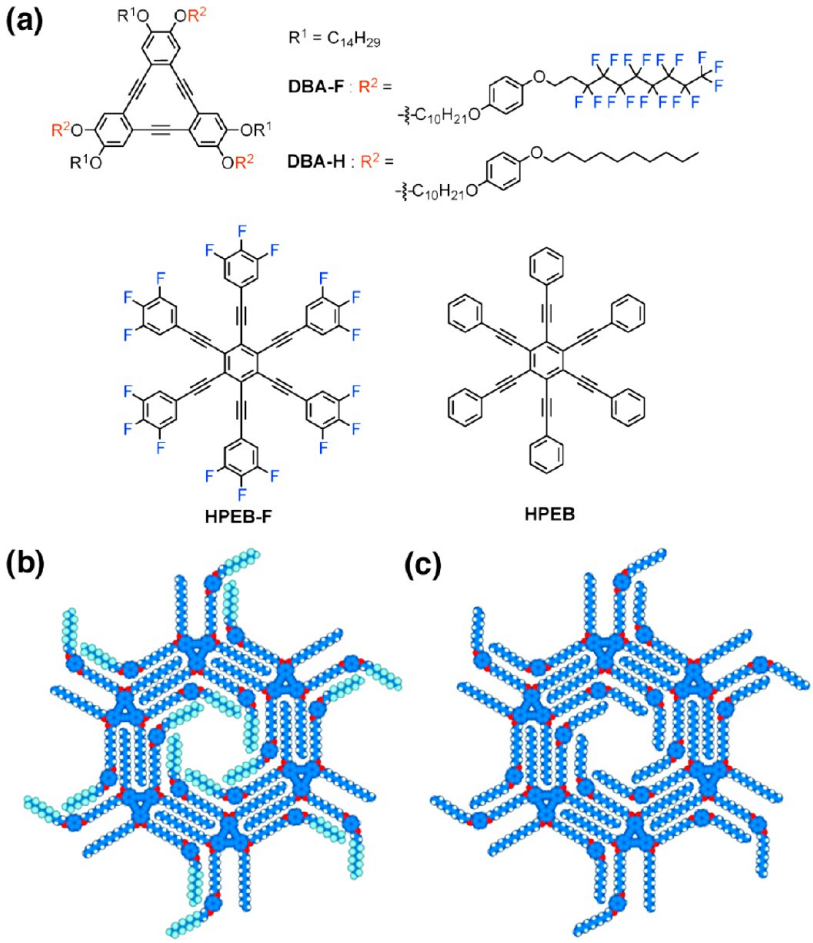

Figure 1. (a) Chemical structures of DBA-F, DBA-H, HPEB-F, and HPEB. (b,c) Molecular models of the honeycomb structures formed by DBA-F and DBA-H, respectively.

dots located at the corners of the hexagonal pores and lines of dim fuzzy rods at the rims of the hexagonal pores correspond to the phenylene linkers and fluoroalkyl chains, respectively. The fuzzy appearance of the fluoroalkyl chains is probably due to their lower tunneling efficiency.[42] Unit cell parameters are $a = b = 5.0 \pm 0.1$ nm and $\gamma = 60 \pm 1°$.

Similar to **DBA-F**, the formation of a honeycomb structure of **DBA-H** was confirmed at the 1-phenyloctane/graphite interface (Figure 2c,d). In the STM image, the phenylene units and alkyl chains placed at the hexagonal pores are clearly visualized. All alkyl chains were parallel to the main symmetry axes of the graphite surface. Unit cell parameters ($a = b = 5.0 \pm 0.1$ nm, $\gamma = 60 \pm 1°$) are identical to those of **DBA-F** because the terminal fluoroalkyl or alkyl chains in the R^2 group are placed at the pores (free spaces) of the honeycomb structures and do not participate in the formation of the intermolecular linkages.

STM Observation of Monolayers Formed by a Mixture of DBA and Guest Molecules. The occupancy ratio of guest molecules at the pores varied as a functional of the composition of the DBA and guest molecules. In the following experiments, the composition was kept at a constant ratio (DBA/guest molecule = 2.4/1.0, concentrations: 3.1×10^{-6} M for DBA and 1.3×10^{-6} M for the guest) because after several trials we found that at this composition and concentration the difference in the guest binding was most clearly observed. Therefore, the guest binding abilities of the decorated pores could be evaluated by the comparison of the percentages of pores that accommodate the guest molecule in the networks.

An STM image of the monolayer prepared from a mixture of **DBA-F** and **HPEB-F** at the 1-phenyloctane/graphite interface is shown in Figure 3a. The formation of a honeycomb structure was observed in which the guest molecule was coadsorbed at some of the pores. On the basis of an appearance of the pore space in the image, the pores were classified into three categories: *bright pores* containing an immobilized guest, *fuzzy pores* with dim bright feature at the center of the pore, and *dark pores* which do not contain any guest (Figure 3b). In the borderline cases between the fuzzy pores and dark pores, where it was not possible to determine from the appearance, pores were classified as *undefined pores*. In Figure 3b and Supporting Information Figure S1, these pores are indicated by red, green, blue, and pink hexagons, respectively.

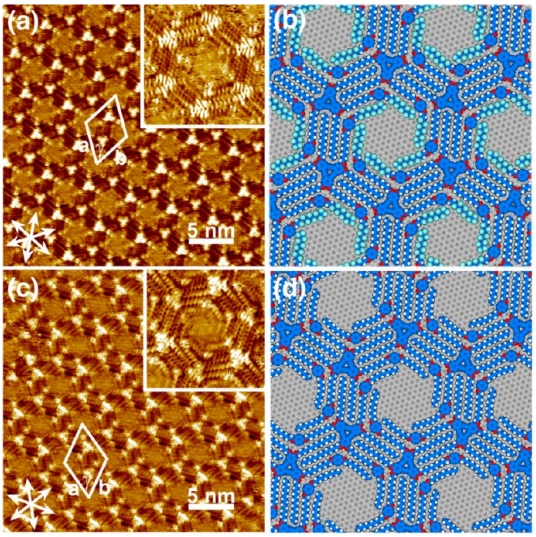

Figure 2. (a,b) STM image and an optimized molecular model of a honeycomb structure of DBA-F formed at the 1-phenyloctane/graphite interface (concentration = 4.4 × 10^{-6} M, tunneling parameters: I_{set} = 0.19 nA and V_{set} = −290 mV). Inset: enlarged image of the hexagonal pore (tunneling parameters: I_{set} = 0.15 nA and V_{set} = −290 mV). (c,d) STM image and an optimized molecular model of a honeycomb structure of DBA-H formed at the 1-phenyloctane/graphite interface (concentration = 2.0 × 10^{-6} M, tunneling parameters: I_{set} = 0.10 nA and V_{set} = −290 mV). Inset: enlarged image of the hexagonal pore (tunneling parameters: I_{set} = 0.08 nA and V_{set} = −180 mV). White arrows indicate the directions of main symmetry axes of underlying graphite. All MM simulations were performed using the COMPASS force field.

To support the classification conducted based on the appearance of the pores, the apparent height of pore space was analyzed.[43−45] The relative heights of the pore space with respect to that of the DBA core as a reference were estimated by averaging the data obtained from more than three height profiles (Figure S1 and the procedure details described in Supporting Information). As a result, the relative heights were 1.14 for the bright pore, 1.08 for the fuzzy pore, and 0.82 for the dark pore. Whereas the heights of the bright and fuzzy pores are nearly the same as that of the DBA core, revealing the presence of the guest molecule in both cases, the relatively low height of the dark pores indicates the absence of the guest. The fuzzy appearance of the guest is attributed to its lateral or rotational dynamics in the pore due to the thermal fluctuation of the guest molecule and/or the peripheral fluoroalkanes. The height profile analyses thus provide support for the classification.

Statistical analysis for 3827 pores from 26 large area STM images (60 nm × 60 nm) for the 2D network of a mixture of **DBA-F** and **HPEB-F** gave the following distributions: bright pores, 20%; fuzzy pores, 36%; dark pores, 40%; undefined pores, 4% (Table 1). The guest molecule was accommodated in 56% of the total pores (sum of the bright and fuzzy pores). The analysis of the distances between the phenylene linkers of **DBA-F**

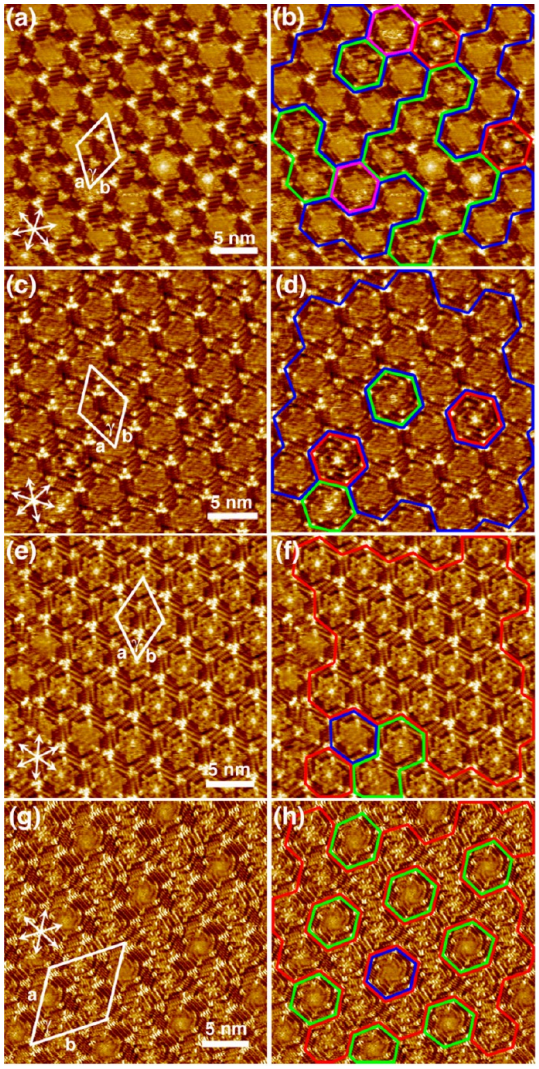

Figure 3. (a,b) STM images of monolayers formed by DBA-F and HPEB-F (concentrations: 3.1 × 10^{-6} M for DBA-F and 1.3 × 10^{-6} M for HPEB-F, tunneling parameters: I_{set} = 185 pA and V_{set} = −290 mV). (c,d) STM images of monolayers formed by DBA-H and HPEB-F (concentrations: 3.1 × 10^{-6} M for DBA-H and 1.3 × 10^{-6} M for HPEB-F, tunneling parameters: I_{set} = 185 pA and V_{set} = −290 mV). (e,f) STM images of monolayers formed by DBA-F and HPEB (concentrations: 3.1 × 10^{-6} M for DBA-F and 1.3 × 10^{-6} M for HPEB, tunneling parameters: I_{set} = 300 pA and V_{set} = −290 mV). (g,h) STM images of monolayers formed by DBA-H and HPEB (concentrations: 1.5 × 10^{-6} M for DBA-H and 3.6 × 10^{-6} M for HPEB, tunneling parameters: I_{set} = 185 pA and V_{set} = −290 mV). Red, green, blue, and pink hexagons indicate the *bright pores* containing an immobilized guest, *fuzzy pores* containing a mobile guest, *dark pores* which do not contain any guest, and *unde®ned pores* categorized between the *fuzzy* and *dark* pores, respectively.

across the corner of the hexagonal pore (corner-to-corner distance) revealed that the sizes of all pores were identical among those of different appearance (3.0 ± 0.1 nm, Table 2). Unit cell parameters are $a = b$ = 5.0 ± 0.1 nm and $\gamma = 60 \pm 1°$.

Figure 3c displays an STM image of the 2D molecular network formed by a mixture of **DBA-H** and **HPEB-F**. In this case, the formation of a honeycomb structure

TABLE 1. Distributions of the Bright, Fuzzy, and Dark Pores

			number of pores counted and its fraction (%)			
DBA[a]	guest[a]	total number of pores analyzed	bright pore	fuzzy pore	dark pore	undefined pore
DBA-F	**HPEB-F**	3827	757 (20%)	1388 (36%)	1521 (40%)	161 (4%)
DBA-H	**HPEB-F**	4320	312 (7%)	379 (9%)	3497 (81%)	132 (3%)
DBA-F	**HPEB**	1855	1199 (65%)	403 (22%)	126 (7%)	127 (7%)
DBA-H	**HPEB**	1607	955 (59%)	500 (31%)	99 (6%)	53 (3%)

[a] In all cases, the concentrations of DBA and guest are 3.1×10^{-6} and 1.3×10^{-6} M, respectively.

TABLE 2. Corner-to-Corner Distances of Pores and Distance between the Centers of Alternating DBA Units around Each Hexagonal Pore

		average corner-to-corner distance[a]		distance between the centers of alternating DBA units		
DBA	guest	bright pore (nm)	other pores (nm)	bright pores (nm)	fuzzy pores (nm)	dark pores (nm)
DBA-F			2.9 ± 0.1[b]			5.0 ± 0.1
DBA-F	**HPEB-F**	3.0 ± 0.1	3.0 ± 0.1	5.0 ± 0.1	5.0 ± 0.1	5.0 ± 0.1
DBA-F	**HPEB**	2.9 ± 0.1	2.9 ± 0.1	5.0 ± 0.1	5.0 ± 0.1	5.0 ± 0.1
DBA-H			2.9 ± 0.1[b]			5.0 ± 0.2
DBA-H	**HPEB-F**	2.8 ± 0.1	2.9 ± 0.2	5.0 ± 0.1	5.0 ± 0.2	5.0 ± 0.1
DBA-H	**HPEB**	2.7 ± 0.2	3.0 ± 0.2	5.0 ± 0.1[c] 4.7 ± 0.1[c]	5.0 ± 0.1	5.0 ± 0.1

[a] The corner-to-corner distance corresponds to the distance between the phenylene linkers at the opposite corners across the hexagonal pore. [b] The size of the dark (free) pores. [c] Two distances were observed.

was also observed with guest molecules coadsorbed in some of the pores. The pores were classified into the same categories described above. From a statistical analysis of 4320 pores from 37 large area images (60 nm × 60 nm), the distribution of the three types of the pores was determined to be 7% for the bright pores (red), 9% for the fuzzy pores (green), 81% for the dark pores (blue), and 3% for the undefined pores (pink), respectively (Figures 3d and S2 and Table 1). The dimensions of all the pores were also found to be the same (2.9 ± 0.1 nm for the average corner-to-corner distance). Unit cell parameters are $a = b = 5.0 \pm 0.1$ nm and $\gamma = 60 \pm 1°$ (Table 2).

The formation of the honeycomb structure with a mixture of the four pores was also observed for a mixture of **DBA-F** and **HPEB** at the 1-phenyloctane/graphite interface (Figure 3e). A statistical analysis of the distribution of the three types of pores based on the evaluation of 1855 pores (17 images) afforded the following results: 65% for the bright pores, 22% for the fuzzy pores, 7% for the dark pores, and 7% for the undefined pores (Figures 3f and S3 and Table 1). Once again, there is no difference in the average corner-to-corner distances among the three pore types (2.9 ± 0.1 nm). Unit cell parameters are $a = b = 5.0 \pm 0.1$ nm and $\gamma = 60 \pm 1°$ (Table 2).

The molecular network formed by a mixture of **DBA-H** and **HPEB** is shown in Figure 3g. The formation of a honeycomb structure was observed with the following distributions of the three pore types: bright pores, 59%; fuzzy pores, 31%; dark pores, 6%; undefined pores, 3% (Figures 3h and S4 and Table 1). Unexpectedly, the locations of the bright pores formed an ordered arrangement within the honeycomb lattice. Namely, the fuzzy, dark, and undefined pores were surrounded by the bright pores, showing a long-range ordering of the bright pores. This long-range periodicity was confirmed by the analysis of the distribution of the nearest-neighbor distances between the pores assigned as the fuzzy, dark, and undefined pores in 12 large area images (60 nm × 60 nm; see Supporting Information for details about periodicity analysis). On the other hand, the positions of the fuzzy and dark pore are random. Careful analysis of the structural differences between the three pore types revealed that the size and shape of the bright pores are different from those of the other pores. The averaged corner-to-corner distance, which is defined by the distance between the phenylene units at the opposite corners across the hexagonal pore, is 2.7 ± 0.2 nm for the bright pores, whereas this distance is 3.0 ± 0.2 nm for the other pores (Table 2). Thus, the bright pores are smaller than the other pores. To clarify the shape of the hexagonal pores, we measured the distance between the centers of alternating DBA units around each hexagonal pore. For the fuzzy and dark pores, all distances were identical (5.1 ± 0.1 and 5.0 ± 0.2 nm, respectively), indicating that the positions of the centers of the DBA cores correspond to the vertices of a regular hexagon. Note, however, that the shapes of the

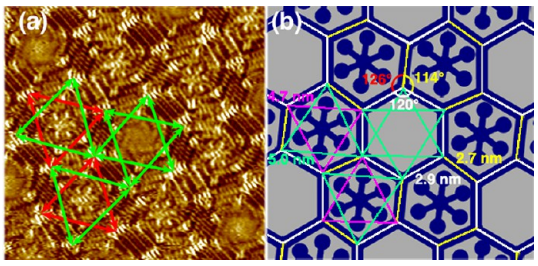

Figure 4. (a) STM image of the superlattice structure formed by DBA-H and HPEB. The red and green double-headed arrows indicate the distances between the centers of alternating DBA cores in the hexagonal networks. The average distances are 5.0 ± 0.1 and 4.7 ± 0.1 nm for red and green arrows, respectively. (b) Schematic representation of a superlattice formed by DBA-H and HPEB. The regular hexagon at the center of the figure is surrounded by six distorted hexagons. The magenta and bright turquoise lines correspond to the next nearest-neighbor distances (4.7 nm and 5.0 nm, respectively) in the regular and distorted hexagons. The angles indicated by white, red, and yellow curved lines are 120°, 126°, and 114°, respectively.

hexagonal pores are not regular hexagon due to the chirality originating from the direction of the interdigitation of the alkyl chains.[40] Though we could not conclude that the fuzzy and dark pores are a regular hexagon on the basis of these distances, we assumed that the fuzzy or dark pores preserve a regular hexagon taking into account the C_6-symmetric nature of the network. Moreover, all angles of these hexagonal pores were *ca.* 120° from the analysis of the images. In comparison, the same analysis for the bright pores revealed two different distances (5.0 ± 0.1 nm for green double-headed arrows and 4.7 ± 0.1 nm for red double-headed arrows in Figure 4a). For the bright pores, the positions of the DBA cores correspond to a hexagon distorted to C_3-symmetry. On the basis of these parameters, we have produced a geometric drawing of the superlattice structure present in the **DBA-H** and **HPEB** network, shown in Figure 4b. The interior angles of the hexagonal pores containing the guests (bright pores) are widened or shortened by *ca.* 6° compared to a regular hexagon. Moreover, the edges of the hexagons shared by two bright pores (yellow lines, 2.7 nm) are slightly shortened by *ca.* 0.2 nm in comparison to the edges between different pore types (white lines, 2.9 nm). The unit cell of the superlattice structure thereby contains three pores, and the parameters are $a = b = 8.6 \pm 0.2$ nm and $\gamma = 60 \pm 1°$.

DISCUSSION

Summary of STM Observations. **DBA-F** and **DBA-H** form honeycomb structures placing the fluoroalkyl or alkyl chains around the perimeter of the hexagonal pores. The guest binding abilities of the functional pores were studied using **HPEB-F** and **HPEB** as guest molecules. By comparing the number of the bright and fuzzy pores to the number of dark and undefined pores (Table 1), it is observed that **HPEB-F** was accommodated in 56 and 16% of the pores formed by **DBA-F** and **DBA-H**, respectively. Conversely, when **HPEB** was used as a guest molecule, the guest occupancy became 87 and 90% for the pores formed by **DBA-F** and **DBA-H** (Table 1). The combination of **DBA-H**/**HPEB** generated an unexpected superlattice structure consisting of a periodic deformation of the hexagonal network. These results are discussed in terms of molecular mechanics simulations and quantum chemical calculations as described below, highlighting the nonbonding interactions and size complementarity between the pore and guest molecule.

Interactions between the Pores and Guest Molecule. In general, the main driving forces for guest coadsorption at surface-confined pores are van der Waals interactions of the guest molecule with the substrate and the surrounding host matrix (the rim of the pore) which operate in a vertical and lateral fashion, respectively.[6−10] In the case of the **DBA-F** network, modification of the pore interior with fluoroalkyl groups is expected to form a fluorous environment. The electronegative nature of the fluorine atoms in the fluoroalkyl group is expected to cause electrostatic interactions with C−H bonds in the guest molecule.[46] To evaluate the strength of these noncovalent intermolecular interactions, we performed MM simulations using the COMPASS force field for models of the network structures placed on a graphene bilayer which represents graphite. Since experimentally no difference was observed for the unit cell parameters of the three host−guest combinations, **DBA-F**/**HPEB-F**, **DBA-F**/**HPEB**, and **DBA-H**/**HPEB-F**, identical periodic boundary conditions were applied ($a = b = 5.08$ nm and $\gamma = 60°$). For comparison, virtual **DBA-H**/**HPEB-H** assembly was also optimized under the same conditions. Note that, because of the use of identical unit cell parameters, the calculated potential energies per mole are proportional to those per unit area (see also Experimental Section for the details). Optimized geometries are displayed in Figure 5, and calculated intermolecular interactions (kcal/mol) and internal energies (kcal/mol) are summarized in Table 3 and Table S2, respectively. In Table 3, E_{total} represents the interaction energy of the entire system consisting of the molecular network of DBA, guest molecules, and the graphite sheet including all intermolecular and molecule−substrate interactions. E_{host} consists of two kinds of interaction energies of the molecular network of DBA on the graphite sheet, one for nonbonding interaction energies of the host network including both intra- and intermolecular interactions and the other for host−substrate interactions, and E_{guest} is the sum of two kinds of interaction energies, an intramolecular nonbonding interactions of the guest molecule in itself without substrate and the interactions between the guest and substrate. From these values, the interaction energies (kcal/mol)

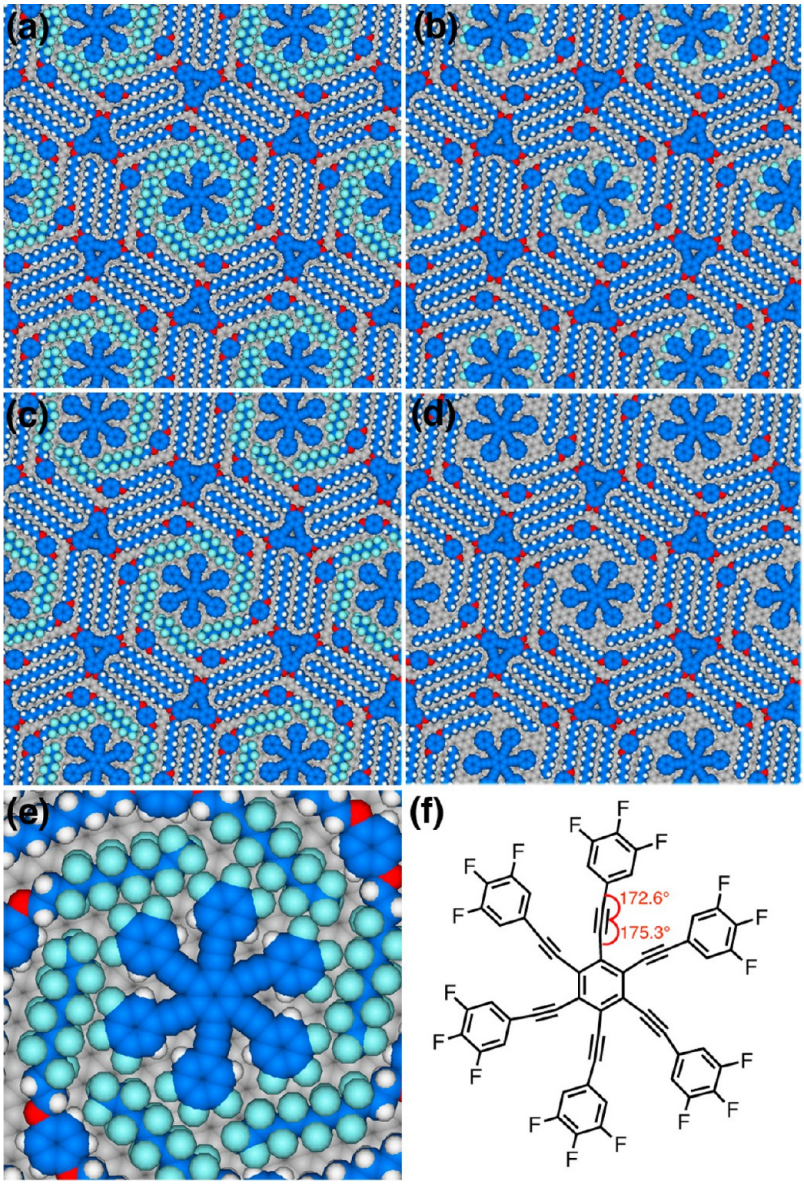

Figure 5. Tentative network models of (a) DBA-F and HPEB-F, (b) DBA-H and HPEB-F, (c) DBA-F and HPEB, and (d) DBA-H and HPEB on a bilayered graphene sheet by molecular mechanics simulations (MM3 parameters) using the experimental unit cell parameters as periodic boundary conditions ($a = b = 5.08$ nm and $\gamma = 60°$). (e) Close-up model for (a) highlighting bent angles of the acetylene unit of HPEB-F. (f) Chemical structure with average bond angles between C(sp^2, central benzene)−C(sp)−C(sp) and C(sp)−C(sp)−C(sp^2, peripheral aryl groups) of the acetylene units. In the case of the DBA-H/HPEB-F combination, the corresponding bond angles of the acetylene units are nearly 180°.

between the host network and guest molecule, $E_{host-guest} = E_{total} - E_{host} - E_{guest}$, were calculated, which are included in Table 3. The $E_{host-guest}$ value for the **DBA-F**/**HPEB-F** pair is the largest of all. Moreover, $E_{host-guest}$ value of the **DBA-F**/**HPEB** pair is larger than that for the **DBA-H**/**HPEB-F** pair. This is consistent with the experimental observation of a lower guest occupation for the **DBA-H**/**HPEB-F** network. The lower proportion of guest binding in the **DBA-F**/**HPEB-F** network as compared to the **DBA-F**/**HPEB** network despite having the most favorable intermolecular interaction energy is attributed to a size complementarity effect as discussed in the following section. Though the smallest $E_{host-guest}$ value was calculated for the **DBA-H**/**HPEB** network, the experimentally observed high proportion of guest binding is attributed to the superlattice formation also as described later.

In order to ascertain the nature of intermolecular interactions between the pore functional group and guest molecule, we performed quantum chemical calculations using pairs of simplified models. Octafluoropropane and propane were employed as models for the functional groups placed around the perimeters of the pores. On the other hand, 1,2,3-trifluorobenzene and benzene were used as models for the peripheral parts of the guest molecules (see Experimental Section for the details). The initial geometries of the pairs were

TABLE 3. Intermolecular Energies for Host–Guest Systems on Bilayered Graphene Sheet Calculated by MM Simulations Using COMPASS Force Field

		intermolecular energy (kcal/mol)[a]					
			host network (E_{host})[b]		guest molecule (E_{guest})[c]		
DBA	guest	whole system (E_{total})	nonbonding interactions without substrate	host–substrate interaction	nonbonding interaction without substrate	guest–substrate interaction	interaction energies between the host and guest molecule ($E_{host-guest}$)[d]
DBA-F	**HPEB-F**	−696.4	79.2	−604.5	−35.6	−112.4	−23.1
DBA-H	**HPEB-F**	−741.8	11.1	−594.9	−33.9	−111.1	−12.9
DBA-F	**HPEB**	−606.2	67.9	−607.0	48.7	−99.2	−16.6
DBA-H	**HPEB**	−685.4	−8.2	−615.7	49.1	−101.3	−9.24

[a] Sum of the intermolecular and molecule–substrate interaction energy. Internal energies are summarized in Table S2. [b] E_{host} values were obtained by single point energy calculations for the host–guest systems in their optimized geometries which do not contain the guest molecules. They consist of the nonbonding interactions without substrate and the host–substrate interactions. To determine the contribution of these parameters, the former energies were elucidated by single point energy calculations for the host–guest systems in their optimized geometries which do not contain the bilayered graphene and the guest molecules. [c] E_{guest} values were obtained by single point energy calculations for the host–guest systems in their optimized geometries which do not contain the host networks. They consist of the nonbonding interactions without substrate and the host–substrate interactions. To determine the contribution of these parameters, the former energies were elucidated by single point energy calculations for the host–guest systems in their optimized geometries which do not contain the bilayered graphene and the host networks. [d] Calculated by the following equation, $E_{host-guest} = E_{total} - E_{host} - E_{guest}$.

set to involve the maximum number of interaction sites between the molecules. The geometries of the pair models were optimized with a C_{2v}-symmetry constraint using the MP2/aug-cc-pVDZ or MP2/aug-cc-pVTZ levels of theory.[47,48] Figure 6 shows optimized geometries of the pair models. The energies of intermolecular interactions were calculated by subtracting the energies of the constituent molecules from that of the corresponding pair model (Table 4). Basis set superposition error was corrected for all calculations using the counterpoise method. The pair of octafluoropropane/1,2,3-trifluorobenzene is calculated to be more stable than the pairs of octafluoropropane/benzene and propane/1,2,3-trifluorobenzene. The interaction energy of the octafluoropropane/benzene pair is larger than that of the propane/1,2,3-trifluorobenzene pair. These results qualitatively agree with the result of the MM simulations. The pair of propane/benzene shows comparable interaction energy to that of the octafluoropropane/1,2,3-trifluorobenzene pair contrary to the prediction by the MM simulations. This contradiction would be attributed to a size mismatch between the pore and guest molecule in the MM simulation, which is discussed in the following section. Next, charge distributions in the optimized geometries were calculated by natural population analysis at the MP2/aug-cc-pVTZ level of theory. The results are shown in Figure 6. For the octafluoropropane/1,2,3-trifluorobenzene pair, the fluorine atoms of both molecules are significantly negatively charged (Figure 6a). This implies that the fluorophilicity due to the dispersion forces between fluorine atoms plays an important role in the stabilization.[24,47−49] By contrast, for the propane/1,2,3-trifluorobenzene and octafluoropropane/benzene

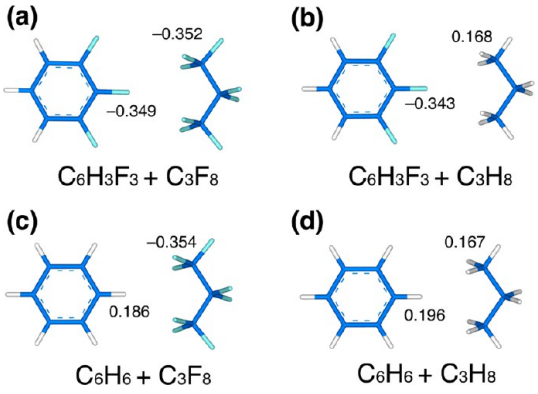

Figure 6. Optimized geometries for the pair models between (a) octafluoropropane and 1,2,3-trifluorobenzene, (b) propane and 1,2,3-trifluorobenzene, (c) octafluoropropane and benzene, and (d) propane and benzene by the MP2 simulations at the aug-cc-pVTZ level of theory. The values at the relevant atoms are the atomic charges calculated by natural population analysis.

pairs, the fluorine atoms are negatively charged, as well, whereas the hydrogen atoms preserve positive charge (Figure 6b,c). The magnitudes of the absolute charge in the latter pair are larger than that of the former, indicating more favorable electrostatic interaction in a fluoroalkane/aromatic C–H pair.[50−53] Moreover, the shortest interatomic distance in the former pair is slightly shorter than that in the latter (Table 4), in support of more favorable electrostatic interaction in the former. In the case of the propane/benzene pair, both hydrogen atoms are positively charged, showing van der Waals interactions (Figure 6d). On the basis of the above analysis, we suggest that the favorable guest binding observed for the combinations of **DBA-F/HPEB-F** and **DBA-F/HPEB** are attributed to fluorophilicity and

TABLE 4. Shortest Interatomic Distances and Interaction Energies for Pair Models by MP2/aug-cc-pVDZ and MP2/aug-cc-pVTZ Calculations

	MP2/aug-cc-pVDZ		MP2/aug-cc-pVTZ[a]	
pair model	shortest interatomic distance (Å)	interaction energy (kcal/mol)[b]	shortest interatomic distance (Å)	interaction energy (kcal/mol)[b]
C_3F_8—$C_6H_3F_3$	3.13	−1.12	3.07	−1.29
C_3H_8—$C_6H_3F_3$	3.03	−0.73	3.01	−0.82
C_3F_8—C_6H_6	2.94	−0.78	2.88	−1.01
C_3H_8—C_6H_6	2.62	−1.24	2.60	−1.36

[a] A larger basis set is preferred to reproduce F···F and F···H interactions as reported in refs 49 and 50. [b] Calculated by subtracting the energies of the constituent molecules from that of the pair model. Basis set superposition error was corrected for all calculations using the counterpoise method.

electrostatic interaction between the host network and guest molecule, respectively.

Effect of Size Complementarity on Guest Binding. In general, size and shape complementarity between guest and pore helps to maximize van der Waals interactions and is a major factor in determining the guest binding ability.[6−10] In the case of the modified DBAs, **DBA-F** and **DBA-H**, the pore sizes should be defined to a certain extent by the alkyl chain length (the inner C_{14} chain and the outer $C_{10}O$-phenylene unit) attached directly to the DBA core. However, the size of the hexagonal pore formed by **DBA-F** should be slightly smaller than that of **DBA-H** (Table 2) because of the larger van der Waals radius of fluorine (1.47 Å) as compared to that of hydrogen (1.27 Å).[54] Indeed, the mean volume of fluoroalkanes is reported to be larger than that of alkanes, with cross sections of 27−30 $Å^2$ for the former and 18−21 $Å^2$ for the latter.[55−59] Similarly, for the guest molecules, the diameter of **HPEB-F** is larger than that of **HPEB**. The longest distances between two terminal atoms estimated for the optimized geometries at the M062x/6-311g(d,p) level of theory are 19.2 and 18.6 Å, respectively.

The **DBA-F**/**HPEB** pair exhibited the best size matching in addition to favorable host−guest interactions showing the largest proportion of guest binding. In the case of the **DBA-F**/**HPEB-F** combination, whereas the size of the pore is the same, the guest size is larger. In the model optimized by the MM simulations, the acetylene units of **HPEB-F** at the pore adopt a distinctly bent geometry (Figure 5e,f) to avoid steric repulsion. Because of this disadvantage, the proportion of guest binding remains small despite the stronger intermolecular interactions between the pore functional groups and guest molecule as a result of the fluorophilicity. Conversely, in the case of the combination of **DBA-H**/**HPEB**, the size of the guest is slightly smaller than that of the pore. Therefore, the pores are deformed and shrink in order to maximize van der Waals interactions with the guest molecule. Note that once the hexagonal angles are expanded at one corner and reduced at the second corner to the same extent to form a C_3-symmetric structure, the third corner should remain at 120° (Figure 4b). Such regular deformation of the hexagonal network results in the formation of the superlattice structure. This unique structural change through an induced-fit mechanism is ascribed to the adaptability of the DBA molecules to adjust the angle with which the alkyl chains are attached to the core.[60] This reveals a dynamic characteristic of the porous self-assembled monolayer formed by DBA derivatives.[61]

From the above discussion, we conclude that the pores of the **DBA-F** and **DBA-H** networks are not enlarged by an induced-fit mechanism[61] in response to a *large* guest molecule because the phenylene linkers at the corners of the pore prevent the slippage of the interdigitated alkyl chains, in marked contrast to the pristine DBAs with linear alkoxy chains of comparable chain length.[62] In response to a *small* guest molecule, however, the pore in the **DBA-F** and **DBA-H** networks can be deformed by changing hexagon angles in a regular manner to maximize intermolecular interactions through an induced-fit mechanism.

CONCLUSIONS

We have designed **DBA-F** and **DBA-H** for the construction of the modified pores with the fluoroalkyl or alkyl chains placed around the perimeter of hexagonal pores. The investigation of the guest binding abilities of the modified pores in the **DBA-F** network using hexakis(phenylethynyl)benzene **HPEB** and its fluoroalkyl cousin **HPEB-F** as guest molecules revealed that the modified pores exhibited guest binding attributed to electrostatic interactions and fluorophilicity between the guests and the (fluoro)alkane groups. This is, to our knowledge, the first example of a noncovalent interaction other than van der Waals forces being utilized in binding to neutral guest molecules at a surface-confined pore. During the course of this study, we have also observed the formation of a superlattice structure formed by a periodic structural deformation of the hexagonal pores of the **DBA-H** network in response to **HPEB** through an induced-fit mechanism. This unique behavior is ascribed to the characteristic adaptability of the modified 2D porous network formed by DBA molecules. The present results provide

a significant insight toward the creation of functional materials on the basis of the surface-confined porous networks and also in the field of 2D crystal engineering in general.

EXPERIMENTAL SECTION

STM Investigation. All experiments were performed at 20–25 °C using a Nanoscope IIIa (Digital Instruments Inc.) with an external pulse/function generator (Agilent 33220A) with negative sample bias. Tips were mechanically cut from Pt/Ir wire (80%/20%, diameter 0.20 or 0.25 mm).

Prior to imaging, DBAs and guest molecules were dissolved in commercially available 1-phenyloctane (TCI) at solute concentrations of *ca.* 10^{-6} M, and a drop of this solution (~8 μL) was applied on a freshly cleaved surface of HOPG (grade ZYB, Momentive Performance Material Quartz Inc., Strongsville, OH). To minimize kinetic effects, the STM images of monolayers formed by a mixture of the host and guest molecules were taken after annealing at 70 °C for 30 min in a sealed sample drying oven. For annealing treatments, a liquid cell (25 μL) placed on the substrate was employed to minimize the effect of solvent evaporation. By changing the tunneling parameters during the STM imaging, namely, the voltage applied to the substrate and the average tunneling current, it was possible to switch from the visualization of the adsorbate layer to that of the underlying HOPG substrate. This enabled us to correct for drift effects by the use of SPIP software (Image Metrology A/S). The white colored axes shown in the figures indicate the directions of the main symmetry axes of graphite underneath the molecular layers.

Molecular Mechanics Simulation. Molecular mechanics simulations were performed with the Materials Studio 5.5 using the Discover module with COMPASS force field.

Each starting structure of **DBA-H**, **DBA-F**, **HPEB**, and **HPEB-F** was built from the respective molecular model whose structure was optimized by the semiempirical PM3 method. Then, the orientation of the alkyl chains relative to the π-system was adjusted based on that observed in the STM images.

The molecules were placed 0.35 nm above the first layer of a periodic two-layer sheet of graphite (interlayer distance of graphite is also 0.35 nm), and the alkyl chains were adjusted to align parallel to the directions of the graphite symmetry axes. The graphite structure was frozen during the simulations, and a cutoff of 2.0 nm was applied for the van der Waals interactions (Lennard-Jones type). All simulations were performed under periodic boundary conditions ($a = b = 5.08$ nm, $c = 10.0$ nm, $\alpha = \beta = 90°$ and $\gamma = 60°$).

Quantum Chemical Calculations. All theoretical calculations were performed with the Gaussian 09 package.[63] The MP2 functional with the aug-cc-pVDZ or aug-cc-pVTZ basis set was used for the geometry optimizations of heteromolecular dimers. Such large basis sets are required to estimate the intermolecular interactions of fluorinated molecules.[47,48] Initial geometries with C_{2v}-symmetric constraints were set to maximize intermolecular interactions between the functional groups. The energies of intermolecular interactions were calculated by subtracting the energies of the constituent molecules from that of the corresponding pair model. Basis set superposition error was corrected for all calculations using the counterpoise method. Natural population analyses (MP2/aug-cc-pVTZ level of theory) were performed for the optimized geometries by the MP2 calculations. The results are summarized in Figure 6 and Table 4. For geometry optimizations of **HPEB** and **HPEB-F**, the M062x functional with the 6-311G(d,p) basis set was used.

Conflict of Interest: The authors declare no competing financial interest.

Acknowledgment. This work is supported by Grants-in-Aid for Scientific Research from the Ministry of Education, Culture, Sports, Science, and Technology, Japan, JST-PRESTO "Molecular technology and creation of new functions", the JSPS Japanese–German Graduate Externship, the Fund of Scientific Research–Flanders (FWO), KU Leuven (GOA 2011/2), and the Hercules Foundation, the Belgian Federal Science Policy Office through IAP 7/05.

Supporting Information Available: Details of experimental procedures, additional STM images, analysis of superlattice periodicity, details of height analysis, details of MM and DFT simulations, and syntheses of DBA derivatives and guest molecule. This material is available free of charge *via* the Internet at http://pubs.acs.org.

REFERENCES AND NOTES

1. Barth, J. V. Molecular Architectonics on Metal Surfaces. *Annu. Rev. Phys. Chem.* **2007**, *58*, 375–407.
2. Bartels, L. Tailoring Molecular Layers at Metal Surface. *Nat. Chem.* **2010**, *2*, 87–95.
3. Barth, J. V.; Costantini, G.; Kern, K. Engineering Atomic and Molecular Nanostructures at Surfaces. *Nature* **2005**, *437*, 671–679.
4. Elemans, J. A. A. W.; Lei, S.; De Feyter, S. Molecular and Supramolecular Networks on Surfaces: From Two-Dimensional Crystal Engineering to Reactivity. *Angew. Chem., Int. Ed.* **2009**, *48*, 7298–7332.
5. Palma, C.-A.; Samorì, P. Blueprinting Macromolecular Electronics. *Nat. Chem.* **2011**, *3*, 431–436.
6. Theobald, J. A.; Oxtoby, N. S.; Phillips, M. A.; Champness, N. R.; Beton, P. H. Controlling Molecular Deposition and Layer Structure with Supramolecular Surface Assemblies. *Nature* **2003**, *424*, 1029–1031.
7. Bonifazi, D.; Mohnani, S.; Llanes-Pallas, A. Supramolecular Chemistry at Interface: Molecular Recognition on Nanopattered Porous Surface. *Chem.—Eur. J.* **2009**, *15*, 7004–7025.
8. Kudernac, T.; Lei, S.; Elemans, J. A. A. W.; De Feyter, S. Two-Dimensional Supramolecular Self-Assembly: Nanoporous Networks on Surfaces. *Chem. Soc. Rev.* **2009**, *38*, 402–421.
9. Zhang, X.-M.; Zeng, Q.-D.; Wang, C. Host–Guest Supramolecular Chemistry at Solid–Liquid Interface: An Important Strategy for Preparing Two-Dimensional Functional Nanostructures. *Sci. China* **2014**, *57*, 13–25.
10. Stepanow, S.; Lingenfelder, M.; Dmitriev, A.; Spillmann, H.; Delvigne, E.; Lin, N.; Deng, X.; Cai, C.; Barth, J. V.; Kern, K. Steering Molecular Organization and Host–Guest Interactions Using Two-Dimensional Nanoporous Coordination Systems. *Nat. Mater.* **2004**, *3*, 229–233.
11. Perdigão, L. M. A.; Saywell, A.; Fontes, G. N.; Staniec, P. A.; Goretzki, G.; Phillips, A. G.; Champness, N. R.; Beton, P. H. Functionalized Supramolecular Arrays for Surface Templating. *Chem.—Eur. J.* **2008**, *14*, 7600–7607.
12. Philips, A. G.; Perdigão, L. M. A.; Beton, P. H.; Champness, N. R. Tailoring Pores for Guest in a Unimolecular Surface Self-Assembled Hydrogen Bonded Network. *Chem. Commun.* **2010**, *46*, 2775–2777.
13. Räisänen, M. T.; Slater, A. G.; Champness, N. R.; Buck, M. Effect of Pore Modification on the Templating of Guest Molecules in a 2D Honeycomb Network. *Chem. Sci.* **2012**, *3*, 84–92.
14. Tahara, K.; Inukai, K.; Adisoejoso, J.; Yamaga, H.; Balandina, T.; Blunt, M. O.; De Feyter, S.; Tobe, Y. Tailoring Surface-Confined Nanopores with Photoresponsive Groups. *Angew. Chem., Int. Ed.* **2013**, *52*, 8373–8376.
15. Ciesielski, A.; Lena, S.; Masiero, S.; Spada, G. P.; Samorì, P. Dynamers at the Solid–Liquid Interface: Controlling the Reversible Assembly/Reassembly Process between Two Highly Ordered Supramolecular Guanine Motifs. *Angew. Chem., Int. Ed.* **2010**, *49*, 1963–1966.
16. El Malah, T.; Ciesielski, A.; Piot, L.; Troyanov, S. I.; Mueller, U.; Weidner, S.; Samorì, P.; Hecht, S. Conformationally Preorganized and pH-Responsive Flat Dendrons: Synthesis

and Self-Assembly at the Liquid–Solid Interface. *Nanoscale* **2012**, *4*, 467–472.
17. Piot, L.; Meudtner, R. M.; El Malah, T.; Hecht, S.; Samorì, P. Modulating Large-Area Self-Assembly at the Solid–Liquid Interface by pH-Mediated Conformational Switching. *Chem.—Eur. J.* **2009**, *15*, 4788–4792.
18. Tahara, K.; Lei, S.; Mamdouh, W.; Yamaguchi, Y.; Ichikawa, T.; Uji-i, H.; Sonoda, M.; Hirose, K.; De Schryver, F. C.; De Feyter, S.; *et al.* Site-Selective Guest Inclusion in Molecular Networks of Butadiyne-Bridged Pyridino and Benzeno Square Macrocycles on a Surface. *J. Am. Chem. Soc.* **2008**, *130*, 6666–6667.
19. Scott, R. L. The Solubility of Fluorocarbons. *J. Am. Chem. Soc.* **1948**, *70*, 4090–4093.
20. Dunlap, R. D.; Bedford, R. G.; Woodbrey, J. C.; Furrow, S. D. Liquid–Vapor Equilibrium for the System: Perfluoro-*n*-hexane-*n*-Hexane. *J. Am. Chem. Soc.* **1959**, *81*, 2927–2930.
21. Young, C. L. Upper Critical Solution Temperature of Perfluoro-*n*-Alkane and *n*-Alkane Mixtures. *Trans. Faraday Soc.* **1969**, *65*, 2639–2644.
22. Mukerjee, P.; Handa, T. Adsorption of Fluorocarbon and Hydrocarbon Surfactants to Air–Water, Hexane–Water, and Perfluorohexane–Water Interfaces. Relative Affinities and Fluorocarbon–Hydrocarbon Nonideality Effects. *J. Phys. Chem.* **1981**, *85*, 2298–2303.
23. Mukerjee, P. Fluorocarbon–Hydrocarbon Interactions in Interfacial and Micellar Systems. *J. Am. Oil Chem. Soc.* **1982**, *59*, 573–578.
24. Binks, B. P.; Fletcher, P. D. I.; Kotsev, S. N.; Thompson, R. L. Adsorption and Aggregation of Semifluorinated Alkanes in Binary and Ternary Mixtures with Hydrocarbon and Fluorocarbon Solvents. *Langmuir* **1997**, *13*, 6669–6682.
25. Dorset, D. L. Binary Phase Behavior of Perfluoroalkanes. *Macromolecules* **1990**, *23*, 894–901.
26. Krafft, M. P.; Riess, J. G. Chemistry, Physical Chemistry, and Uses of Molecular Fluorocarbon–Hydrocarbon Diblocks, Triblocks, and Related Compounds—Unique "Apolar" Components for Self-Assembled Colloid and Interface Engineering. *Chem. Rev.* **2009**, *109*, 1714–1792.
27. Nguyen, H. T.; Sigaud, G.; Achard, M. F.; Hardouin, F.; Twieg, R. J.; Betterton, K. Rod-like Mesogens with Antipathetic Fluorocarbon and Hydrocarbon Tails. *Liq. Cryst.* **1991**, *10*, 389–396.
28. Chiang, Y. H.; Ames, A. E.; Gaudiana, R. A.; Adams, T. G. Study of Tails in Smectic Liquid Crystals. I. The Effect of Fluorocarbon/Hydrocarbon Ether Tails on Phenyl Ester Biphenyl Cores. *Mol. Cryst. Liq. Cryst.* **1991**, *208*, 85–98.
29. Dahn, U.; Erdelen, C.; Ringsdorf, H.; Festag, R.; Wendorff, J. H.; Heiney, P. A.; Maliszewskyj, N. C. Fluoroalkylated Discotic Liquid Crystals. *Liq. Cryst.* **1995**, *19*, 759–764.
30. Clark, C. G., Jr.; Floudas, G. A.; Lee, Y. J.; Graf, R.; Spiess, H. W.; Müllen, K. Molecularly Tethered Amphiphiles as 3-D Supramolecular Assembly Platforms: Unlocking a Trapped Conformation. *J. Am. Chem. Soc.* **2009**, *131*, 8537–8547.
31. Percec, V.; Johansson, G.; Ungar, G.; Zhou, J. Fluorophobic Effect Induces the Self-Assembly of Semifluorinated Tapered Monodendrons Containing Crown Ethers into Supramolecular Columnar Liquid Crystalline Phase. *J. Am. Chem. Soc.* **1996**, *118*, 9855–9866.
32. Ishikawa, Y.; Kuwahara, H.; Kunitake, T. Self-Assembly of Bilayer Membranes in Organic Solvents by Novel Amphiphilic Compounds. *J. Am. Chem. Soc.* **1989**, *111*, 8530–8531.
33. Sato, S.; Iida, J.; Suzuki, K.; Kawano, M.; Ozeki, T.; Fujita, M. Fluorous Nanodroplets Structurally Confined in an Organopalladium Sphere. *Science* **2006**, *313*, 1273–1276.
34. Gesquière, A.; Abdel-Mottaleb, M. M.; De Schryver, F. C.; Sieffert, M.; Müllen, K. Imaging of a Fluorine-Substituted Isophthalic Acid Derivatives on Graphite with Scanning Tunneling Microscopy. *Langmuir* **1999**, *15*, 6821–6824.
35. Abdel-Mottaleb, M. M. S.; De Feyter, S.; Sieffert, M.; Klapper, M.; Müllen, K.; De Schryver, F. C. *In Situ* Investigation of Dynamical Nanophase Separation. *Langmuir* **2003**, *19*, 8256–8261.
36. Tahara, K.; Furukawa, S.; Uji-i, H.; Uchino, T.; Ichikawa, T.; Zhang, J.; Mamdouh, W.; Sonoda, M.; De Schryver, F. C.; De Feyter, S.; *et al.* Two-Dimensional Porous Molecular Networks of Dehydrobenzo[12]annulene Derivatives *via* Alkyl Chain Interdigitation. *J. Am. Chem. Soc.* **2006**, *128*, 16613–16625.
37. Lei, S.; Tahara, K.; De Schryver, F. C.; Van der Auweraer, M.; Tobe, Y.; De Feyter, S. One Building Block, Two Different Supramolecular Surface-Confined Patterns: Concentration in Control at the Solid–Liquid Interface. *Angew. Chem., Int. Ed.* **2008**, *47*, 2964–2968.
38. Blunt, M. O.; Adisoejoso, J.; Tahara, K.; Katayama, K.; Van der Auweraer, M.; Tobe, Y.; De Feyter, S. Temperature-Induced Structural Phase Transitions in a Two-Dimensional Self-Assembled Network. *J. Am. Chem. Soc.* **2013**, *135*, 12068–12075.
39. Tahara, K.; Lei, S.; Adisoejoso, J.; De Feyter, S.; Tobe, Y. Supramolecular Surface-Confined Architectures Created by Self-Assembly of Triangular Phenylene-Ethynylene Macrocycles *via* van der Waals Interaction. *Chem. Commun.* **2010**, *46*, 8507–8525.
40. Tahara, K.; Yamaga, H.; Ghijsens, E.; Inukai, K.; Adisoejoso, J.; Blunt, M. O.; De Feyter, S.; Tobe, Y. Control and Induction of Surface-Confined Homochiral Porous Molecular Networks. *Nat. Chem.* **2011**, *3*, 714–719.
41. Lazzaroni, R.; Calderone, A.; Lambin, G.; Rabe, J. P.; Brédas, J. L. A Theoretical Approach to the STM Imaging of Adsorbates on the Graphite Surface. *Synth. Met.* **1991**, *41*, 525–528.
42. Faglioni, F.; Claypool, C. L.; Lewis, N. S.; Goddard, W. A., III. Theoretical Description of the STM Images of Alkanes and Substituted Alkanes Adsorbed on Graphite. *J. Phys. Chem. B* **1997**, *101*, 5996–6020.
43. Tersoff, J.; Hamann, D. R. Theory and Application for the Scanning Tunneling Microscopy. *Phys. Rev. Lett.* **1983**, *50*, 1998–2001.
44. Bumm, L. A.; Arnold, J. J.; Dunbar, T. D.; Allara, D. L.; Weiss, P. S. Electron Transfer through Organic Molecules. *J. Phys. Chem. B* **1999**, *103*, 8122–8127.
45. Sakano, T.; Higashiguchi, K.; Matsuda, K. Comparison of Molecular Conductance between Planar and Twisted 4-Phenylpyridines by Means of Two-Dimensional Phase Separation of Tetraphenylporphyrin Templates at a Liquid–HOPG Interface. *Chem. Commun.* **2011**, *47*, 8427–8429.
46. Mu, Z.; Shu, L.; Fuchs, H.; Mayor, M.; Chi, L. Two-Dimensional Chiral Networks Emerging from the Aryl–F···H Hydrogen-Bond-Driven Self-Assembly of Partially Fluorinated Rigid Molecular Structures. *J. Am. Chem. Soc.* **2008**, *130*, 10840–10841.
47. Tsuzuki, S.; Uchimaru, T.; Mikami, M.; Urata, S. Magnitude and Orientation Dependence of Intermolecular Interaction between Perfluoroalkanes: High Level *Ab Initio* Calculations of CF_4 and C_2F_6 Dimers. *J. Chem. Phys.* **2002**, *116*, 3309–3315.
48. Tsuzuki, S.; Uchimaru, T.; Mikami, M.; Urata, S. Magnitude and Orientation Dependence of Intermolecular Interaction of Perfluoropropane Dimer Studied by High-Level *Ab Initio* Calculations: Comparison with Propane Dimer. *J. Chem. Phys.* **2004**, *121*, 9917–9924.
49. Huque, F. T. T.; Jones, K.; Saunders, R. A.; Platts, J. A. Statistical and Theoretical Studies of Fluorophilicity. *J. Fluorine Chem.* **2002**, *115*, 119–128.
50. Shimoni, L.; Glusker, J. P. The Geometry of Intermolecular Interactions in Some Crystalline Fluorine-Containing Organic Compounds. *Struct. Chem.* **1994**, *5*, 383–397.
51. Howard, J. A. K.; Hoy, V. J.; O'Hagan, D.; Smith, G. T. How Good Is Fluorine as a Hydrogen Bond Acceptor? *Tetrahedron* **1996**, *52*, 12613–12622.
52. Dunitz, J. D. Organic Fluorine: Odd Man Out. *ChemBioChem* **2004**, *5*, 614–621.
53. Tsuzuki, S.; Uchimaru, T.; Mikami, M.; Urata, S. *Ab Initio* Calculations of Intermolecular Interaction of CHF_3 Dimer: Origin of Attraction and Magnitude of CH/F Interaction. *J. Phys. Chem. A* **2003**, *107*, 7962–7968.
54. Bondi, A. van der Waals Volumes and Radii. *J. Phys. Chem.* **1964**, *68*, 441–451.

55. Gang, O.; Ellmann, J.; Möller, M.; Kraack, H.; Sirota, E. B.; Ocko, B. M.; Deutsch, M. Surface Phases of Semi-fluorinated Alkane Melts. *Europhys. Lett.* **2000**, *49*, 761–767.
56. Ocko, B. M.; Wu, X. Z.; Sirota, E. B.; Sinha, S. K.; Gang, O.; Deutsch, M. Surface Freezing in Chain Molecules: Normal Alkanes. *Phys. Rev. E* **1997**, *55*, 3164–3182.
57. Barton, S. W.; Goudot, A.; Bouloussa, O.; Rondelez, F.; Lin, B.; Novak, F.; Acero, A.; Rice, S. A. Structural Transition in a Monolayer of Fluorinated Amphiphile Molecule. *J. Chem. Phys.* **1992**, *96*, 1343–1351.
58. Li, M.; Acero, A. A.; Huang, Z.; Rice, S. A. Formation of an Ordered Langmuir Monolayer by a Non-polar Chain Molecule. *Nature* **1994**, *367*, 151–153.
59. Takiue, T.; Vollhardt, D. Miscibility of Alkanol and Fluoroalkanol in Langmuir Film at the Air/Water Interface. *Colloids Surf., A* **2002**, *198−200*, 797–804.
60. Ghijsens, E.; Ivasenko, O.; Tahara, K.; Yamaga, H.; Itano, S.; Balandina, T.; Tobe, Y.; De Feyter, S. A Tale of Tails: Alkyl Chain Directed Formation of 2D Porous Networks Reveals Odd-Even Effects and Unexpected Bicomponent Phase Behavior. *ACS Nano* **2013**, *7*, 8031–8042.
61. Furukawa, S.; Tahara, K.; De Schryver, F. C.; Van der Auweraer, M.; Tobe, Y.; De Feyter, S. Structural Transformation of a Two-Dimensional Molecular Network in Response to Selective Guest Inclusion. *Angew. Chem., Int. Ed.* **2007**, *46*, 2831–2834.
62. Lei, S.; Tahara, K.; Feng, X.; Furukawa, S.; De Schryver, F. C.; Müllen, K.; Tobe, Y.; De Feyter, S. Molecular Clusters in Two-Dimensional Surface-Confined Nanoporous Molecular Networks: Structure, Rigidity, and Dynamics. *J. Am. Chem. Soc.* **2008**, *130*, 7119–7129.
63. Frisch, M. J.; Trucks, G. W.; Schlegel, H. B.; Scuseria, G. E.; Robb, M. A.; Cheeseman, J. R.; Scalmani, G.; Barone, V.; Mennucci, B.; Petersson, G. A.; *et al. Gaussian 09*, revision C.1; Gaussian, Inc.: Wallingford, CT, 2009.